arXiv:1411.3088v1 [cond-mat.mes-hall] 12 Nov 2014

Spin-dependent Refraction at the Atomic Step of Transition-metal Dichalcogenides

Tetsuro Habe and Mikito Koshino
Department of Physics, Tohoku University, Sendai 980-8578, Japan
(Dated: November 13, 2014)

We theoretically propose a novel spin-dependent electronic transport mechanism in which the spin-unpolarized electron beam is split into different directions depending on spins at an atomic domain boundary in non-magnetic material. Specifically, we calculate the electronic transmission across a boundary between monolayer and bilayer of the transition metal dichalcogenide, and demonstrate that up-spin and down-spin electrons entering the boundary are refracted and collimated to opposite directions. The phenomenon is attributed to the strong spin-orbit interaction, the trigonally-warped Fermi surface, and the different crystal symmetries between the monolayer and bilayer systems. The spin-dependent refraction suggests a potential application for a spin splitter, which spatially separates up-spin and down-spin electrons simply by passing the electric current through the boundary.

PACS numbers: 72.25.Dc,73.63.Bd,85.35.Ds

Spin-dependent electron transport is a key ingredient in spintronics which exploits the spin degree of freedom for electronic devices. Particularly, the capability to manipulate spins purely by electric means is a desirable property, as it allows the combination with the conventional electronics. For the electrical control of spins without resorting to magnetic field, the spin-orbit interaction plays an essential role. A variety of spin-dependent transport mechanisms in non-magnetic materials, such as the spin-Hall effect[1] and the spin field effect devices[2], are derived from the spin-orbit interaction.

In this paper, we theoretically propose a novel spin-dependent transport mechanism, referred to as spin-dependent refraction in the following, in which the spin-unpolarized electron beam is split into different directions depending on spins at an atomic domain boundary in non-magnetic material. Specifically, we consider an atomic step between monolayer and bilayer of the transition metal dichalcogenide (TMD) as shown in Figure 1(a) and demonstrate that up-spin and down-spin electrons entering from the bilayer side are refracted and collimated to opposite directions, as illustrated in Fig. 1(b). The spin-dependent refraction effect can be exploited for a spin splitter, which spatially separates up-spin and down-spin electrons simply by passing the electric current through the boundary, just like an optical refraction separating a light beam by the wavelength.

TMD recently attracts a significant attention as a novel family of two-dimentional material.[3–9] A hallmark of the electronic structure of the TMD monolayer is the correlation of the spin and valley degrees of freedom. Specifically, the valence band maxima located at K and K' valleys are spin split in the opposite direction between the two valleys as shown in Fig. 2, and this is due to the strong spin-orbit coupling of the heavy transition-metal atoms and also the absence of the inversion symmetry in the lattice structure. The spin-valley correlated band structure leads to characteristic spin-dependent optical properties, which have been extensively studied in the recent years.[10–17]. The properties of TMD atomic layers are also studied in terms of the electric and spintronic transport[18–23].

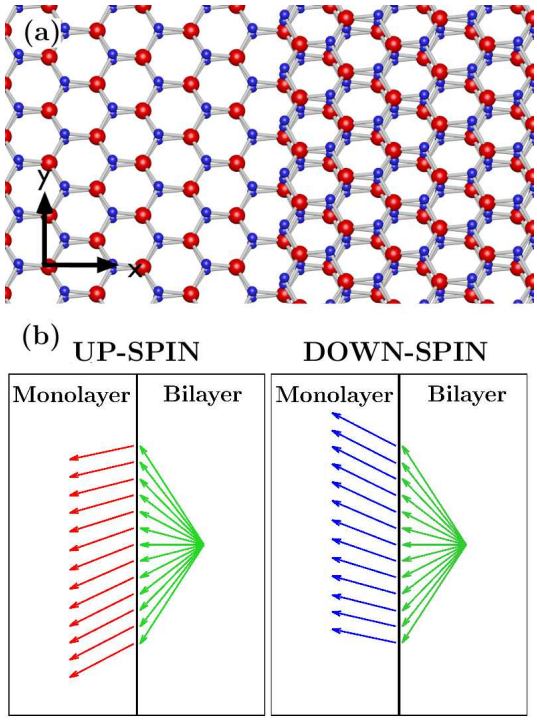

FIG. 1. (a) Atomic structure of the junction between the monolayer and bilayer of TMD. The large (red) and small (blue) spheres represent the transition-metal and chalcogenide atoms, respectively. (b) Electron refraction at the atomic step between monolayer and bilayer of $MoTe_2$ for an incident electron from the bilayer side.

Here we propose the spin-dependent refraction as a mechanism to manipulate the electronic spins in TMD without using optics or magnetic field. We calculate the electronic transmission probability across the monolayer-bilayer boundary on several kinds of TMDs using the tight-binding model based on the first-principle band calculation, and actually show that the up-spin and down-spin electrons are refracted different angles at the bound-

ary. The phenomenon is attributed to the common characteristics of TMDs; the strong spin-orbit interaction, the trigonal warped Fermi surface, and the difference of the symmetry between the monolayer and bilayer TMDs. We find that the spin-dependent refraction effect is conspicuous in TMDs MX_2 with M = Mo, W and X = Se, Te, while it is not observed in the sulphides (X=S), where the carriers are fully reflected at the atomic step. Previously, the electron transmission property was studied for graphene monolayer-bilayer junction[24], and it was shown that the electrons are refracted to different angles depending on K and K' valleys. In TMDs, a valley-dependent transport immediately leads to a spin-dependent transport, owing to the spin-valley correlation.

We consider an atomic junction between monolayer and bilayer of a single sort of TMD, as shown in Fig. 1. Here we assume that one layer in the bilayer region is truncated at the y axis (zigzag direction), and the other layer continues to the monolayer region. The bilayer region takes the inversion-symmetric structure called 2H stacking, which is the most common phase in the bulk TMD. We also assume that the carrier density in the sample is controlled by a single gate electrode underneath and it is homogeneous over the whole system. To simulate this situation, we appropriately differentiate the electrostatic potential of the monolayer and that of the bilayer to achieve the given carrier density at the common Fermi energy. To describe the motion of electrons, we perform the first-principle calculation using the numerical package of quantum-ESPRESSO[25], and obtain the electronic structure of infinite TMD monolayer and that of bilayer. From the obtained first-principle electronic density, we compute the maximally-localized Wannier function using Wannier90 package[26] and derive the tight-binding hopping parameters for bulk monolayer and bilayer. Finally, we apply the tight-binding model to the monolayer-bilayer junction to calculate the transmission probability with the Green's function method.[27] In the first principle calculations, we adopt the geometrical parameters for the crystal structure in Refs. 28–30, and employ the GGA pseudopotentials, the cutoff energy of the plane-wave basis 150[eV] and the convergence criterion of 10^{-8}[eV]. The basis of the tight-binding Hamiltonian consists of d-orbitals on transition-metal atoms and p-orbitals on chalcogenide atoms. The detailed description of the tight-binding Hamiltonian for monoalyer-bilayer junction is presented in Appendix.

Fig. 2 presents the first-principle band structures of the monolayer and bilayer of MoS_2, $MoSe_2$, and $MoTe_2$. In the monolayer of each TMD, the valence band is spin-split near the peaks at K and K', where the spin is polarized to the opposite directions in two valleys.[31] In the bilayer, on the other hand, the energy bands are completely spin-degenerate due to the inversion symmetry of the lattice structure. We also notice that the valence band at the Γ point becomes relatively higher in bilayer than in monolayer. In MoS_2 bilayer, the Γ point is higher

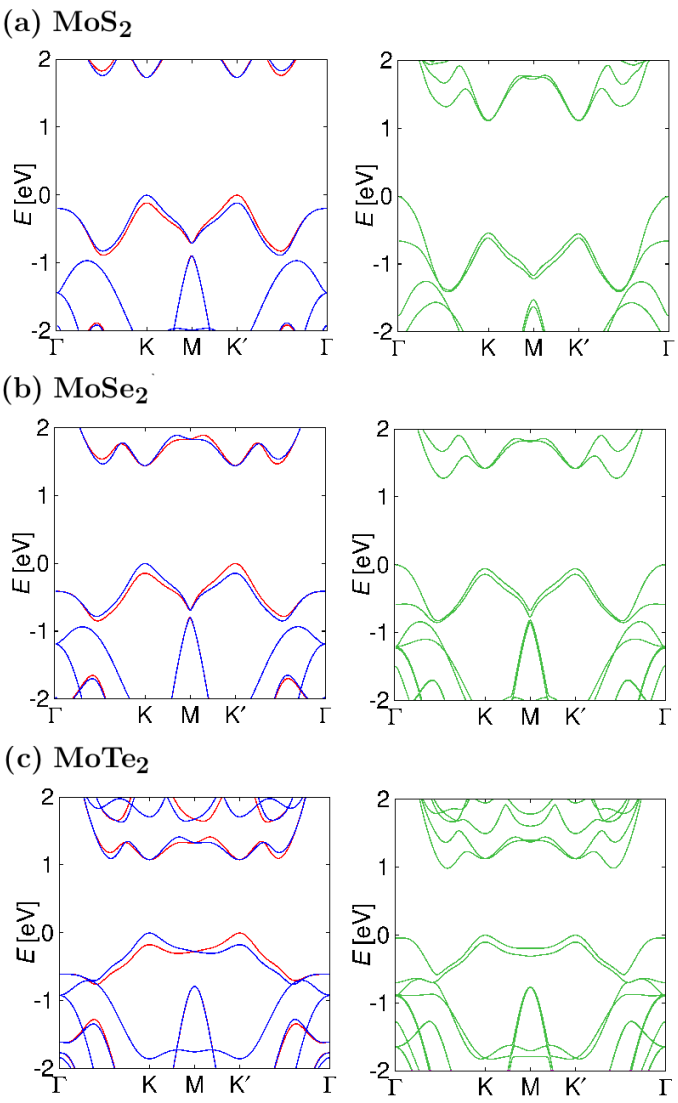

FIG. 2. Band structures of monolayer (left) and bilayer (right) of (a)MoS_2, (b)$MoSe_2$, and (c)$MoTe_2$. In monolayer, the up-spin and down-spin states are represented by the red and blue lines, respectively. In bilayer, the two spin states are degenerate.

than the K and K' points by about 500meV, while in $MoSe_2$ bilayer the deference reduces to 100[meV], and in $MoTe_2$ bilayer, the Γ point is slightly lower than the K and K'. The band structures of the tungsten dichalchogenides WX_2 (not shown) exhibit a similar tendency where the Γ point energy becomes relatively lower for heavier chalcogenide atoms.[28,32]

Now let us consider a TMD monoalyer-bilayer hybrid system. In Fig. 3, we present some example of the calculated spin-dependent electron transmission in the monolayer-bilayer junction of hole-doped $MoTe_2$ at the electron density of $n = -7.02 \times 10^{13}\mathrm{cm}^{-2}$. We first consider a situation where an incident electron comes from the monolayer region with the initial angle θ_m, and

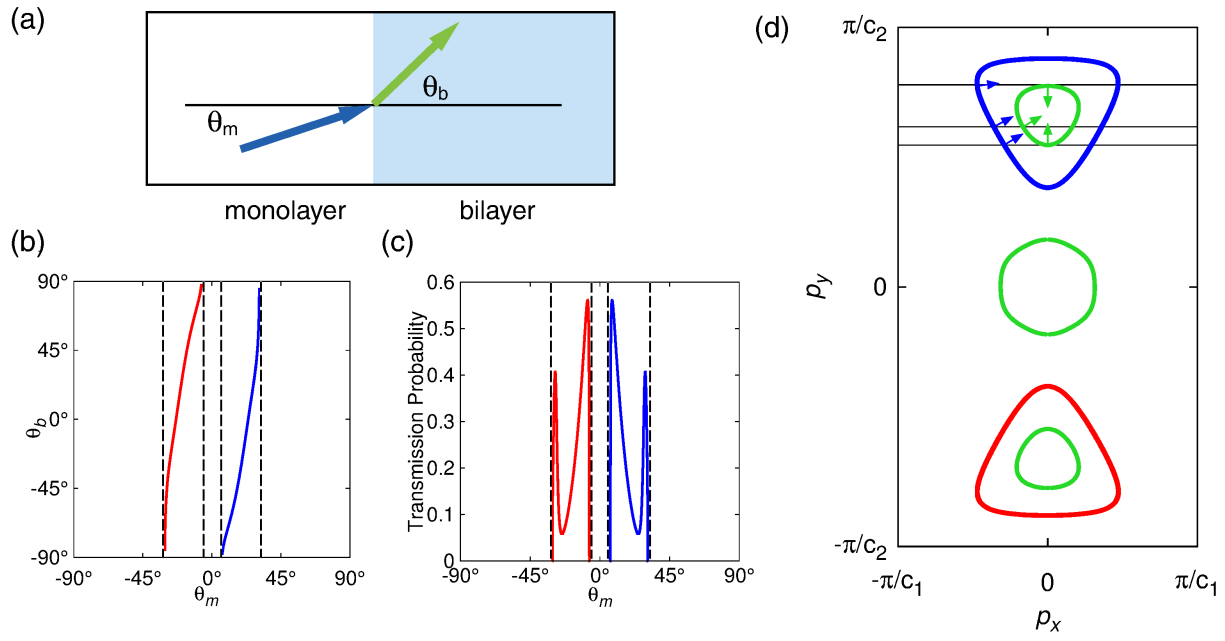

FIG. 3. Transmission property in the monolayer-bilayer junction of $MoTe_2$ with the carrier density $n = -7.02 \times 10^{13}[\mathrm{cm}^{-2}]$. (a) Schematic of the refraction process with the definition of the θ_m and θ_b. (b) Relation between the velocity angles θ_m and θ_b, for up-spin (red) and the down-spin (blue) electrons. (c) Corresponding transmission probability as a function of θ_m. (d) Fermi surfaces of the monolayer and bilayer. The red and blue curves represent up-spin and down-spin states in monolayer, respectively, and the green is the spin-degenerate states in bilayer. Arrows indicate the velocities of the electrons at some p_y's on the Fermi surface.

transmitted to the bilayer region with the finial angle θ_b, as shown in Fig.3(a). Here we adopt the electron picture rather than the hole picture in describing the carrier transmission although the system is hole-doped. The traveling angle is defined by $\theta = \arctan(v_y/v_x)$ from the expectation value of the velocity (v_x, v_y) of the corresponding electronic state. In Fig. 3(b), the relation between the initial and final angles is plotted separately for up-spin and down-spin electrons. The corresponding transmission probability is plotted in Fig. 3(c) as a function of the incident angle θ_m. Since the system is time-reversal symmetric, Fig. 3(b) can be inversely viewed as the angle relationship (with spin inverted) for an electron coming from the bilayer region with the initial angle θ_b and transmitted to monolayer region with the final angle θ_m. Fig. 3(c) then represents the transmission probability as a function of the final angle θ_m.

Fig. 3(b) shows that the atomic step is highly angle-selective for an incident carrier from the monolayer side, i.e. it allows to pass an up-spin electron only within a narrow range of angle $-30^\circ \lesssim \theta_m \lesssim -7^\circ$, and down-spin electron only within $7^\circ \lesssim \theta_m \lesssim 30^\circ$, while the transmitted carriers widely spread in $-90^\circ < \theta_b < 90^\circ$ in the bilayer region. If an electron comes from the bilayer region, on the contrary, any incident angles can be allowed while the transmitted electrons are highly collimated in the monolayer to the different angle ranges depending on spins.

The spin-dependent refraction is attributed to the difference in the Fermi surface structure between the monolayer and bilayer TMDs, which are illlustrated in Fig. 3(d). The monolayer's Fermi surface is completely spin-split, and the up-spin and down-spin branches are located at K' and K points, respectively. On the other hand, the bilayer's Fermi surface is completely spin degenerate, and also it has the third pocket at Γ point besides K and K'. Due to the condition of a homogeneous carrier density, the total area enclosed by the Fermi surfaces is exactly equal in monolayer and bilayer. As a consequence, the size of the K and K' pockets are significantly smaller in the bilayer than in the monolayer, because in bilayer, the Fermi surface is doubled due to the spin degeneracy and also the area of the Γ pocket reduces the share of K and K'.

Because of the translation symmetry in the y axis, the transverse momentum p_y is preserved in the transmission process. The change of the traveling angle can be found by comparing the velocity vectors (normal to the Fermi surface) of the monolayer and bilayer states sitting at the same p_y. As shown in Fig. 3(d), the smaller Fermi surface of the bilayer restricts the corresponding monolayer region to a portion of the whole Fermi surface, in which the velocity direction varies only slightly due to the trigonal warped character of the equi-energy surface. This explains the reason why monolayer's electrons within only a small angle range can transmit to the

bilayer region. As the up-spin (K') and down-spin (K) Fermi surfaces are mirror symmetric about the x axis, the up-spin and down-spin electrons are refracted in the opposite direction with respect to $\theta = 0$, as shown in Fig. 3(c).

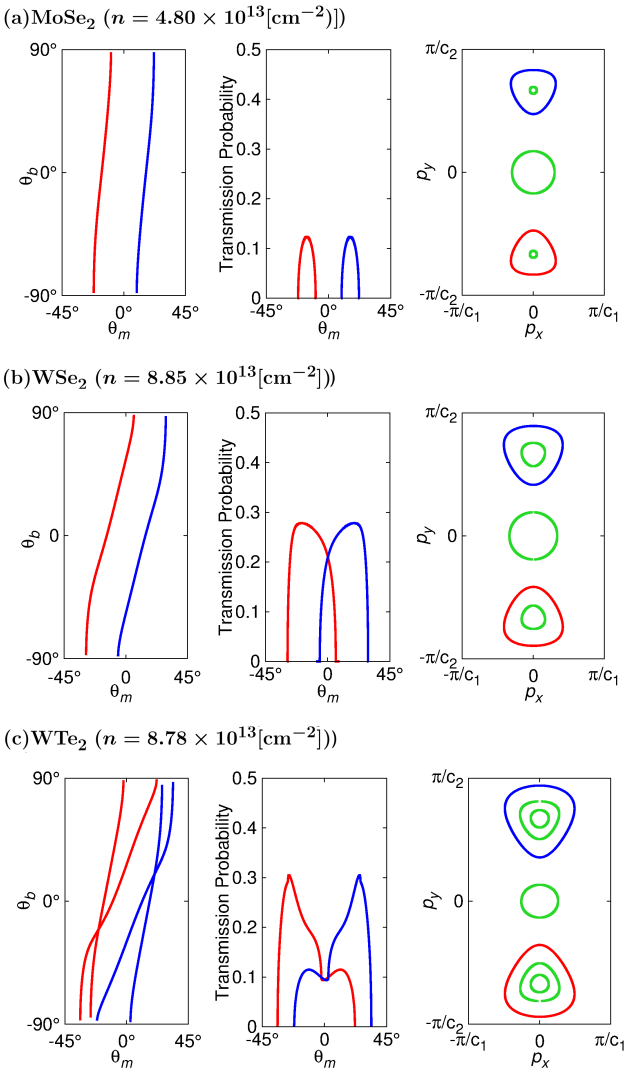

FIG. 4. Similar plots to Fig. 3 for (a)$MoSe_2$, (b)WSe_2, and (c)WTe_2.

The carrier density assumed in Fig. 3 was chosen in such a way that the Fermi energy comes slightly above the lower branch of the spin-split valence bands of the monolayer $MoTe_2$. This is the maximum hole density (i.e., the lowest Fermi energy) under the condition that each of K and K' valleys is dominated by a single spin. If we raise the Fermi energy toward the valence band maximum, the difference in the refraction angle between up and down spins gradually decreases. This is because the Fermi surface becomes more circular near the band edge (i.e., the trigonal warping is weaker) so that the transmission becomes more symmetric with respect to $\theta = 0$, and that reduces the spin dependence of the transmission.

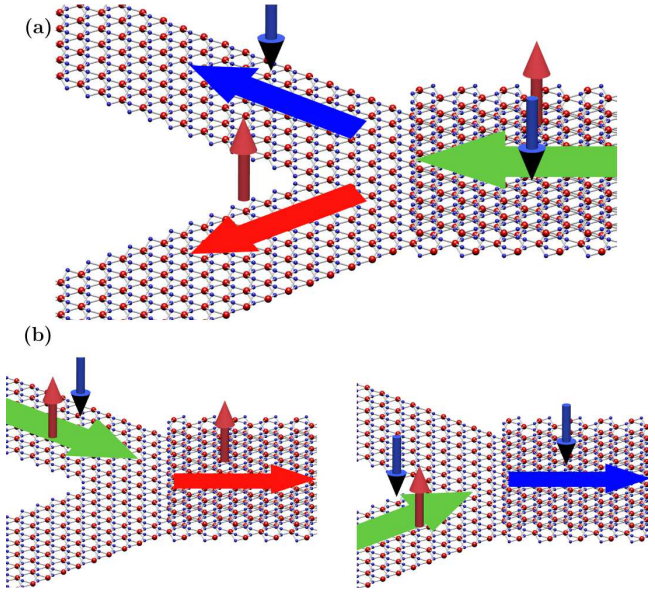

FIG. 5. Spin filtering effect in Y-junction fabricated on the monolayer-bilayer boundary of hole-doped TMD, for the electron beam injected from (a) the bilayer region and (b) the monolayer region.

Fig. 4 presents similar calculations for other TMDs, $MoSe_2$, WSe_2, and WTe_2. We see that those materials share a basically similar characteristics of the Fermi surface and the nature of the spin-dependent refraction. In the transition-metal disulfides MS_2 (not shown), on the other hand, the valence electrons are completely reflected at the atomic step, because the low-energy spectrum of the bilayer is dominated by Γ point, and the transmission from K and K' points of the monolayer side is completely blocked due to the momentum mismatch.

We can exploit the atomic step on TMD as a spin splitter which spatially separates up-spin and down-spin electrons, simply by passing the electric current through the boundary. For example, we can consider a Y-shaped junction fabricated on monolayer-bilayer boundary of hole-doped TMDs as shown in Fig. 5, where a single strip in the bilayer region forks into two branches in the monolayer region. If the spin-unpolarized electric current is injected from the bilayer side, it separates into the up-spin and down-spin currents in different branches of the monolayer due to the spin-dependent collimation effect, as shown in Fig. 5(a). When the spin-unpolarized current is put from one of the monolayer branches, on the contrary, only a single spin can enter the bilayer region [Fig. 5(b)], because of the spin and angle selective transmission from the monolayer region.

To conlcude, we studied the electron transmission at the monolayer-bilayer atomic step of TMDs, and find the spin-dependent refraction effect which separates the up-spin and down-spin carriers into different traveling directions. The phenomena suggest a potential application for the spintronic devices which transfers the spin informa-

tion into the electric information.

We would like to thank Professor Takashi Koretsune for his help in using the quantum-ESPRESSO and Wannier90 packages. This work was supported by Grants-in-Aid for Scientific research (GrantsNo. 24740193 and No. 25107005). Wannier90: A Tool for Obtaining Maximally-Localised Wannier Functions A. A. Mostofi, J. R. Yates, Y.-S. Lee, I. Souza, D. Vanderbilt and N. Marzari Comput. Phys. Commun. 178, 685 (2008) [ONLINE JOURNAL]

Appendix A: Tight-binding model for the monolayer-bilayer junction

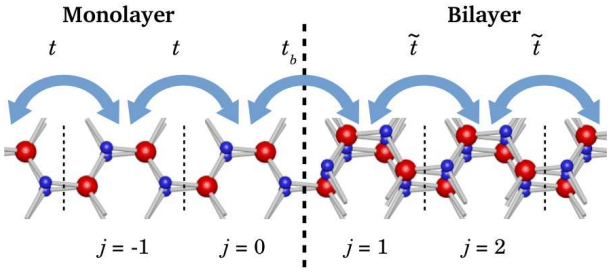

FIG. 6. Tight-binding model for the TMD monolayer-bilayer junction. Red and blue spheres represent transition-metal and chalcogenide atoms, resprectively. Unit cells in the monolayer (bilayer) contain two (four) transition-metal atoms and four (eight) chalcogenide atoms.

Figure 6 schemtically illustrates the tight-binding model for the TMD monolayer-bilayer junction. The system is translationally symmetric in the y direction, so that it is reduced to a one-dimensional system labeled by the momentum p_y. The unit cell of monolayer (bilayer) region contains two (four) transition-metal atom and four (eight) chalcogenide atoms. Note that the unit cell here is twice as large as the primitive unit cell of the bulk TMD because of the armchair geometry. We consider five d-orbitals for each transition-metal atom and three p-orbitals for each chalcogenide atom, which sum up to 22 (44) orbitals per spin in monolayer (bilayer) unit cell. The hopping parameters of the tight-binding model are derived by computing the maximally localized Wannier Functions by applying Wannier90 to the first principle electronic density. First we construct the spin-less tight-binding model neglecting the spin-orbit interaction, and introduce the spin-orbit coupling by adding the appropriate $\mathbf{L}\cdot\mathbf{s}$ term to the transition-metal atoms.[33] The up-spin and down-spin states (with respect to z axis) are completely decoupled even in presence of the spin-orbit coupling, and therefore we can calculate the transmission probability for each spin state separately.

The tight-binding Hamiltonian for the monolayer-bilayer junction for given p_y and spin state $s =\uparrow,\downarrow$ is written as

$$\begin{aligned} H(p_y,s) = &\sum_{j\le 0}\left[\boldsymbol{c}_j{}^\dagger h \boldsymbol{c}_j + (\boldsymbol{c}_j{}^\dagger t^\dagger \boldsymbol{c}_{j-1} + \text{h.c.})\right] \\ &+ \left(\tilde{\boldsymbol{c}}_1^\dagger t_b{}^\dagger \boldsymbol{c}_0 + \text{h.c.}\right) \\ &+ \sum_{1\le j}\left[\tilde{\boldsymbol{c}}_j^\dagger \tilde{h}\tilde{\boldsymbol{c}}_j + (\tilde{\boldsymbol{c}}_{j+1}^\dagger \tilde{t}^\dagger \tilde{\boldsymbol{c}}_j + \text{h.c.})\right]. \end{aligned}$$

Here the index j indicates the cell position, where $j\le 0$ and $j\ge 1$ correspond to the monolayer and bilayer regions, respectively. The vector $\boldsymbol{c}_j$ ($j\le 0$) is the $N(=22)$-component annihilation operator of electron at the cell j in the monolayer region, where each component correspond to the atomic orbital inside the unit cell. Similarly, $\tilde{\boldsymbol{c}}_j$ ($j\ge 1$) the $2N$-component annihilation operator for the bilayer region. $h(\tilde{h})$ and $t(\tilde{t})$ are $N\times N(2N\times 2N)$ matrices, where $h(\tilde{h})$ describes the matrix elements inside the unit cell and $t(\tilde{t})$ describes the matrix elements between neighboring cells in the monolayer (bilayer) region. The hopping between monolayer and bilayer regions (i.e., between $j=0$ and 1) is described by t_b, which is $N\times 2N$ matrix. In this paper, we assume that t_b is equivalent to the half submatrix of $\tilde{t}$, i.e., we borrow all the hopping parameters from bulk bilayer and neglect the non-existing upper layer in the monolayer side. We can safely neglect further hopping elements between j and $j+n\,(n\ge 2)$, which are sufficiently small.

[1] J. E. Hirsch, Phys. Rev. Lett. **83**, 1834 (1999).
[2] S. Datta and B. Das, Appl. Phys. Lett. **56**, 665 (1990).
[3] K. F. Mak, C. Lee, J. Hone, J. Shan, and T. F. Heinz, Phys. Rev. Lett. **105**, 136805 (2010).
[4] A. Splendiani, L. Sun, Y. Zhang, T. Li, J. Kim, C.-Y. Chim, G. Galli, and F. Wang, Nano. Lett. **10**, 1271 (2010).
[5] J. N. Coleman, M. Lotya, A. O'Neill, S. D. Bergin, P. J. King, U. Khan, K. Young, A. Gaucher, S. De, R. J. Smith, I. V. Shvets, S. K. Arora, G. Stanton, H.-Y. Kim, K. Lee, G. T. Kim, G. S. Duesberg, T. Hallam, J. J. Boland, J. J. Wang, J. F. Donegan, J. C. Grunlan, G. Moriarty, A. Shmeliov, R. J. Nicholls, J. M. Perkins, E. M. Grieveson, K. Theuwissen, D. W. McComb, P. D. Nellist, and V. Nicolosi, Science **331**, 568 (2011).
[6] Y.-H. Lee, X.-Q. Zhang, W. Zhang, M.-T. Chang, C.-T. Lin, K.-D. Chang, Y.-C. Yu, J. T.-W. Wang, C.-S. Chang, L.-J. Li, and T.-W. Lin, Adv. Mater. **24**, 2320 (2012).
[7] Q. H. Wang, K. Kalantar-Zadeh, A. Kis, J. N. Coleman, and M. S. Strano, Nat. Nano. **7**, 699 (2012).
[8] M. Chhowalla, H. S. Shin, G. Eda, L.-J. Li, K. P. Loh, and H. Zhang, Nat. Chem. **5**, 263 (2013).
[9] W. Jin, P.-C. Yeh, N. Zaki, D. Zhang, J. T. Sadowski, A. Al-Mahboob, A. M. van der Zande, D. A. Chenet, J. I.

Dadap, I. P. Herman, P. Sutter, J. Hone, and R. M. Osgood, Phys. Rev. Lett. **111**, 106801 (2013).
[10] T. Cao, G. Wang, W. Han, H. Ye, C. Zhu, J. Shi, Q. Niu, P. Tan, E. Wang, B. Liu, and J. Feng, Nature Commun. **3**, 887 (2012).
[11] H. Zeng, J. Dai, W. Yao, D. Xiao, and X. Cui, Nat. Nano. **7**, 490 (2012).
[12] K. F. Mak, K. He, J. Shan, and T. F. Heinz, Nat. Nano. **7**, 494 (2012).
[13] H. Shi, H. Pan, Y.-W. Zhang, and B. I. Yakobson, Phys. Rev. B **87**, 155304 (2013).
[14] A. Molina-Sánchez, D. Sangalli, K. Hummer, A. Marini, and L. Wirtz, Phys. Rev. B **88**, 045412 (2013).
[15] R. Suzuki, M. Sakano, Y. J. Zhang, R. Akashi, D. Morikawa, A. Harasawa, K. Yaji, K. Kuroda, K. Miyamoto, T. Okuda, K. Ishizaka, R. Arita, and Y. Iwasa, Nat. Nano. **9**, 611 (2014).
[16] C. Zhang, H. Wang, W. Chan, C. Manolatou, and F. Rana, Phys. Rev. B **89**, 205436 (2014).
[17] M. Yamamoto, S. T. Wang, M. Ni, Y.-F. Lin, S.-L. Li, S. Aikawa, W.-B. Jian, K. Ueno, K. Wakabayashi, and K. Tsukagoshi, ACS Nano **8**, 3895 (2014).
[18] Y. Song and H. Dery, Phys. Rev. Lett. **111**, 026601 (2013).
[19] H. Yuan, X. Wang, B. Lian, H. Zhang, X. Fang, B. Shen, G. Xu, Y. Xu, S.-C. Zhang, H. Y. Hwang, and Y. Cui, Nat. Nano. **advance online publication** (2014), 10.1038/nnano.2014.188.
[20] W. Feng, Y. Yao, W. Zhu, J. Zhou, W. Yao, and D. Xiao, Phys. Rev. B **86**, 165108 (2012).
[21] J. Klinovaja and D. Loss, Phys. Rev. B **88**, 075404 (2013).
[22] A. Kormányos, V. Zólyomi, N. D. Drummond, and G. Burkard, Phys. Rev. X **4**, 011034 (2014).
[23] L. Peng, K. Yao, S. Zhu, Y. Ni, F. Zu, S. Wang, B. Guo, and Y. Tian, J. Appl. Phys. **115**, 223705 (2014).
[24] T. Nakanishi, M. Koshino, and T. Ando, Phys. Rev. B **82**, 125428 (2010).
[25] P. Giannozzi, S. Baroni, N. Bonini, M. Calandra, R. Car, C. Cavazzoni, D. Ceresoli, G. L. Chiarotti, M. Cococcioni, I. Dabo, A. Dal Corso, S. de Gironcoli, S. Fabris, G. Fratesi, R. Gebauer, U. Gerstmann, C. Gougoussis, A. Kokalj, M. Lazzeri, L. Martin-Samos, N. Marzari, F. Mauri, R. Mazzarello, S. Paolini, A. Pasquarello, L. Paulatto, C. Sbraccia, S. Scandolo, G. Sclauzero, A. P. Seitsonen, A. Smogunov, P. Umari, and R. M. Wentzcovitch, J. Phys.: Condens. Matter **21**, 395502 (2009).
[26] A. A. Mostofi, J. R. Yates, Y.-S. Lee, I. Souza, D. Vanderbilt, and N. Marzari, Computer Physics Communications **178**, 685 (2008).
[27] T. Ando, Phys. Rev. B **44**, 8017 (1991).
[28] W. S. Yun, S. W. Han, S. C. Hong, I. G. Kim, and J. D. Lee, Phys. Rev. B **85**, 033305 (2012).
[29] L. Debbichi, O. Eriksson, and S. Lebègue, Phys. Rev. B **89**, 205311 (2014).
[30] J. He, K. Hummer, and C. Franchini, Phys. Rev. B **89**, 075409 (2014).
[31] D. Xiao, G.-B. Liu, W. Feng, X. Xu, and W. Yao, Phys. Rev. Lett. **108**, 196802 (2012).
[32] A. Kumar and P. K. Ahluwalia, Modelling Simul. Mater. Sci. Eng. **21**, 065015 (2013).
[33] G.-B. Liu, W.-Y. Shan, Y. Yao, W. Yao, and D. Xiao, Phys. Rev. B **88**, 085433 (2013).